EUROPEAN ORGANIZATION FOR NUCLEAR RESEARCH

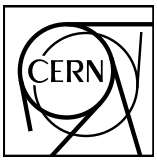

CERN-EP–2021-xxx
May 22, 2023

Observation of abnormal suppression of $f_0(980)$ production in p–Pb collisions at $\sqrt{s_{NN}}$ = 5.02 TeV

Abstract

The multiplicity dependence of $f_0(980)$ production in p–Pb collisions at $\sqrt{s_{NN}} = 5.02$ TeV with ALICE is reported. The production of $f_0(980)$ is measured via the $f_0(980) \rightarrow \pi^+\pi^-$ decay channel in a midrapidity region of $-0.5 < y < 0$. Particle yield ratios of $f_0(980)$ to π and $K^*(892)^0$ are found to be decreasing with an increasing charged-particle multiplicity. The yield ratios of $f_0(980)$ as a function of its transverse momentum (p_T) exhibit a particle-species-dependent behavior. Furthermore, the nuclear modification factor Q_{pPb} (R_{pPb} in centrality intervals, due to the possible bias in the determination of centrality) is measured in various multiplicity ranges. The Q_{pPb} shows strong suppression in the p_T region up to about 4 GeV/c. The results of the particle yield ratios and Q_{pPb} for $f_0(980)$ may help to understand the late hadronic phase in p–Pb collisions and the nature of the internal structure of $f_0(980)$ particles.

1 Introduction

Light scalar mesons, whose spin and parity are zero and even, respectively, are of particular interest as their nature can be explained with an exotic structure [1]. Among them, the understanding of $f_0(980)$ particles lies in a long-standing puzzle in terms of its quark content [2–4]. The $f_0(980)$ is suggested to be a conventional $q\bar{q}$ [5], compact tetraquark [6], or $K\overline{K}$ molecule [7]. In order to analyse the unknown structure of $f_0(980)$, several approaches are accessible in relativistic heavy-ion collisions in conjunction with the information in proton–proton (pp) collisions.

The theory of strong interaction, quantum chromodynamics (QCD), predicts the formation of a state of strongly interacting matter, the so called quark-gluon plasma (QGP), in the hot and dense system reached in relativistic heavy-ion collisions. Many observations at the Large Hadron Collider (LHC), such as flow modulations [8, 9], jet quenching [10], and nuclear modification factors [11], support the existence of the QGP [12]. Specifically, the nuclear modification factors for different particle species in heavy-ion collisions show that the transverse momentum (p_{T}) distribution of particles is strongly modified due to the presence of the hot and dense QGP medium. However, the nuclear modification factors are measured as close to unity in p–A collisions [13] for minimum-bias (MB) events, stating no substantial modification in p–A collisions in the high p_{T} range (> 8 GeV/c).

The relative production yield of particles containing strange quarks is reported to increase faster than those with up and down quarks, which is usually referred to as "strangeness enhancement" [14] in high-multiplicity pp and p–Pb collisions. The observation of the strangeness enhancement, along with measurements of flow modulations in small collision systems [15, 16], may hint at the formation of QGP droplets in small systems. The study of relative production yield for $f_0(980)$ can be useful to check the strange quark content [17, 18] inside $f_0(980)$. On the other hand, the nuclear modification factors for baryons exhibit a strong enhancement at intermediate p_{T} ($2 < p_{\mathrm{T}} < 5$ GeV/c) compared with those for mesons which is mainly due to the number of constituent quarks (NCQ) [19, 20]. In addition, it has been suggested that the elliptic flows of different particles depend on the NCQ as demonstrated in Ref. [21]. These approaches can help to constrain the number of quarks forming $f_0(980)$.

The short-lived resonances, such as $\rho(770)^0$ [22], $K^*(892)^0$ [23, 24], $\Sigma(1385)^{\pm}$ [25], and $\Lambda(1520)$ [26] as well as $f_0(980)$, are good probes to study the properties of the system that results from the hadronisation of a QGP [27]. In the late stage of the evolution of the system formed in heavy-ion collisions, there are two important temperatures and corresponding timescales: the chemical freeze-out, when the inelastic collisions among the constituents are expected to cease, and the later kinetic freeze-out, when all (elastic) interactions stop [28]. Because the duration between the chemical to the kinetic freeze-outs of the system is comparable with the lifetime of resonances [29, 30], the particles originating from those decays can actively interact with the hadronic gas via rescattering and regeneration processes, and such interactions result in modifications of resonance yields. The modifications can be observed by comparing the yield of resonances with those of long-lived or ground-state particles [31]. Measurements of ρ/π and K^*/K yield ratios are good examples to study the properties of the late hadronic phase after the chemical freeze-out. Recently, system-size-dependent suppressions of particle yields are also observed in small systems [23], suggesting rescattering and regeneration processes in small systems. The observation of the modification for the $f_0(980)$ yield may contribute to further understanding of the late hadronic phase.

In this paper, multiplicity-dependent measurement of anomalous suppression of $f_0(980)$ production in p–Pb collisions at $\sqrt{s_{\mathrm{NN}}} = 5.02$ TeV is reported for the first time. The measurement of $f_0(980)$ is conducted at midrapidity ($-0.5 < y < 0$) in $0 < p_{\mathrm{T}} < 8$ GeV/c for different multiplicity classes. In Sec. 2, the experimental setup is described, while the reconstruction of $f_0(980)$ and the relative corrections are explained in Sec. 3. The study of systematic uncertainties for the measurement is reported in Sec. 4. In Sec. 5, p_{T} spectra, particle yield ratios, and the nuclear modification factors are discussed. Finally, model comparisons and conclusions are described in Sec. 6.

2 Experimental setup

The MB events in p–Pb collisions at $\sqrt{s_{\rm NN}}$ = 5.02 TeV used for the present analysis were recorded using the ALICE detector in 2016. The center-of-mass reference system in p–Pb collisions is shifted by $\Delta y_{\rm cms} = 0.465$ units of rapidity along the direction of the proton beam. In the following, the convention that y stands for $y_{\rm cms}$ is used. The ALICE apparatus used during the LHC Run 2 is described in detail in [32]. The present analysis is carried out using the following detectors: V0 [33], the Zero Degree Calorimeters (ZDC) [34], the Inner Tracking System (ITS) [35], the Time Projection Chamber (TPC) [36], and the Time-Of-Flight (TOF) [37].

The V0 detector is an hodoscope of scintillators, located on both sides relative to the interaction point (IP), consisting of V0A and V0C, each made of 32 plastic scintillator strips, covering the full azimuthal angle within the pseudorapidity intervals $2.8 < \eta < 5.1$ and $-3.7 < \eta < -1.7$, respectively. The MB events are selected with a signal given by a hit in both the V0A and V0C in p–Pb collisions. The V0A on the Pb-going side provides the multiplicity class using the sum of the V0A signals at the same time. The collected MB sample corresponds to an integrated luminosity of 0.24 nb^{-1} [38]. The ZDC in p–Pb collisions detects nucleons emitted from the colliding nucleus by nuclear de-excitation processes or knocked out from wounded nucleons, the so called "slow" nucleons. Two identical sets of the ZDC, each composed by a neutron (ZN) and a proton (ZP) calorimeters, are located at 112.5 m from the ALICE IP, on both sides, covering very forward rapidity regions. The ZDC provides the least biased centrality selection in p–Pb collisions [39].

The primary vertex position is reconstructed using the measured track segments in the Silicon Pixel Detector (SPD) [40], the innermost two layers of the ITS. The primary vertex along the beam direction ($z_{\rm vtx}$) is required to be in $|z_{\rm vtx}| < 10$ cm from the nominal point ($z_{\rm vtx} = 0$). The distance between the primary vertex and an additional vertex is requested to be larger than 0.8 cm to reduce the pile up. In addition, the correlations between track candidates measured using different detectors are used to reject the pile up. The probability of pileup events is expected to be about 0.5% in MB events. The TPC is the main tracking detector of ALICE. The TPC covers the pseudorapidity range $|\eta| < 0.9$ over the full azimuth in a uniform solenoidal magnetic field of 0.5 T along the beam axis. The TPC is able to reconstruct charged particles down to $p_{\rm T} = 0.15$ GeV/c. Particle identification (PID) can be performed with the TPC and TOF. The TPC measures ionization energy loss $\mathrm{d}E/\mathrm{d}x$ of charged tracks to separate particle species. The TOF helps particle identification by measuring the flight time of charged particles from the primary vertex to the TOF.

3 Data analysis

$\mathrm{f}_0(980)$ particles are reconstructed via the decay channel of $\mathrm{f}_0(980) \rightarrow \pi^+\pi^-$, where the branching ratio is reported to be B.R. = $46 \pm 6\%$ [41]. Each charged pion reconstructed in the TPC is required to have $p_{\rm T} > 0.15$ GeV/c and $|\eta| < 0.8$ for a uniform detector acceptance. The reconstructed tracks are required to satisfy the standard selection criteria, as reported in [42], to guarantee that only tacks with high quality are selected. To ensure good track momentum resolution, the reconstructed tracks are required to have at least 70 reconstructed points (out of a maximum of 159) in the TPC and two hits in the ITS, with at least one in the SPD. Selection criteria dependent on $p_{\rm T}$ are applied to the distance of closest approach to the primary vertex in the transverse (d_z) and longitudinal (d_{xy}) directions, requiring $d_z < 2$ cm and $d_{xy} < (0.0105 + 0.0350 \times p_{\rm T}^{-1.1})$ cm, respectively, to suppress contamination from secondary charged particles originating from weakly decaying hadrons and interactions with material.

The identification of charged pions is performed using the combined information of the TPC and TOF. The difference between the measured ionization energy loss and the prediction of the Bethe-Bloch parameterization obtained assuming the particle is a pion is required to be within two standard deviations for the pion identification in the TPC. The difference between the measured time-of-flight of the particle

and the time expected for a pion is required to be within three standard deviations to identify as pions using the TOF. The TOF signal is not used for particle identification when it is not originated from the reconstructed track. In this case, the TPC is used for the identification as a standalone detector.

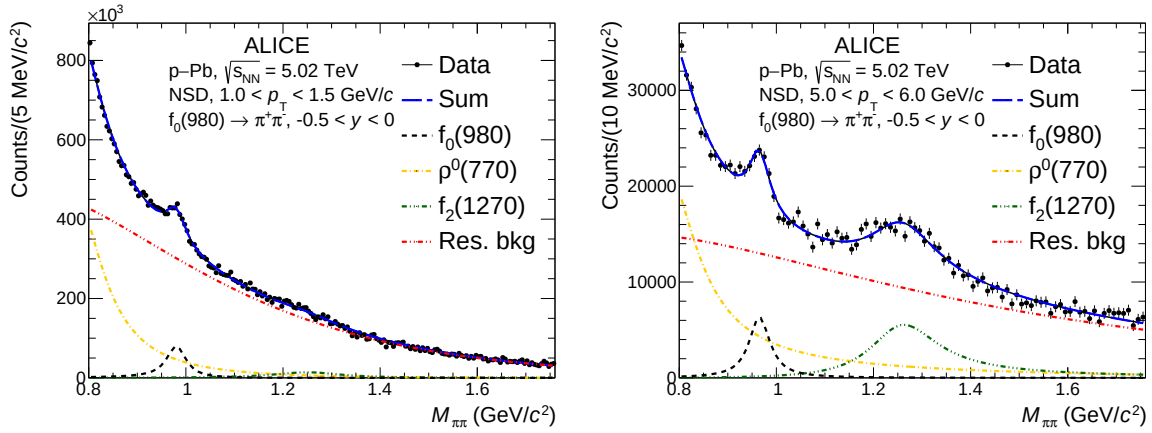

Fig. 1: Invariant mass distribution of $\pi^+\pi^-$ pairs in $-0.5 < y < 0$ after the like-sign background subtraction in p–Pb collisions at $\sqrt{s_{\rm NN}}$ = 5.02 TeV. The left (right) plot is obtained at low (high) $p_{\rm T}$ of $\pi^+\pi^-$ pairs in non-single diffraction (NSD) events.

The $f_0(980)$ signals are extracted using the invariant mass analysis by associating two opposite-charge pions in the same event at $-0.5 < y < 0$ [43]. The combinatorial backgrounds are subtracted using the like-sign method [44]. The like-sign background is constructed as the geometric average of $\pi^+\pi^+$ and $\pi^-\pi^-$ distributions, $2\sqrt{N_{\pi^+\pi^+}N_{\pi^-\pi^-}}$. After subtracting the like-sign backgrounds from the $\pi^+\pi^-$ distribution, peaks of resonances decaying to $\pi^+\pi^-$ can be identified. Figure 1 shows the like-sign-subtracted $\pi^+\pi^-$ invariant mass distributions for $1.0 < p_{\rm T} < 1.5$ GeV/c ($5.0 < p_{\rm T} < 6.0$ GeV/c) in MB events on the left (right) plot. Because $\rho(770)$ and $f_2(1270)$ dominantly decay to $\pi^+\pi^-$ and have large widths, $f_0(980)$ signals are overlapped with contributions from those two resonances. Residual backgrounds ($f_{\rm bkg}$) are mainly attributed to misidentified particles and mini-jets, which are represented as red-dashed-dotted lines in Fig. 1. Each resonance contribution is described with a relativistic Breit-Wigner function (rBW) [22, 42]. Note that detector resolution is expected to give a negligible contribution in the estimate of the widths of broad resonances. The rBW can be expressed as

$$\mathrm{rBW}(M_{\pi\pi}) = \frac{AM_{\pi\pi}\Gamma(M_{\pi\pi})M_0}{(M_{\pi\pi}^2 - M_0^2)^2 + M_0^2\Gamma^2(M_{\pi\pi})}, \tag{1}$$

where $\Gamma(M_{\pi\pi})$ is defined as

$$\Gamma(M_{\pi\pi}) = \left[\frac{(M_{\pi\pi}^2 - 4m_\pi^2)}{(M_0^2 - 4m_\pi^2)}\right]^{(2J+1)/2} \times \frac{\Gamma_0 M_0}{M_{\pi\pi}}. \tag{2}$$

Here, A and M_0 are the amplitude of the rBW and the rest mass of the resonance, respectively. The rest width of the resonance, the spin, and the charged pion mass of 139.5 MeV/c^2 are represented as Γ_0, J, and m_π, respectively. The spins for $f_0(980)$, $\rho(770)$, and $f_2(1270)$ are 0, 1, and 2, respectively. The $f_{\rm bkg}$ is fitted with a Maxwell-Boltzmann-like distribution, which can be expressed as [45]

$$f_{\rm bkg}(M_{\pi\pi}) = B(M_{\pi\pi} - 2m_\pi)^n \exp\left(c_1 M_{\pi\pi} + c_2 M_{\pi\pi}^2\right), \tag{3}$$

where, B, n, c_1, and c_2 are free parameters. Each rBW of the resonance is corrected for the $\pi\pi$ interference [22], which can be expressed as

$$\mathrm{PS}(M_{\pi\pi}) = \frac{M_{\pi\pi}}{\sqrt{M_{\pi\pi}^2 + p_{\rm T}^2}} \times \exp\left(-\sqrt{M_{\pi\pi}^2 + p_{\rm T}^2}/T_{\rm kin}\right), \tag{4}$$

where p_{T} in the above equation denotes the transverse momentum of the $\pi\pi$ pair, and T_{kin} is the kinetic freeze-out temperature and set to be 160 MeV [22] for different multiplicity classes.

The signal extraction carefully considers the width of the $\mathrm{f}_0(980)$ as the width is not yet constrained by measurements ($10 < \Gamma_0^{\mathrm{f}_0} < 100$ MeV/c^2 [1]). The total fit function consists of the sum of three rBWs, one for each resonance, and one function for the background, f_{bkg}. This function has 9 free parameters: 3 for $\mathrm{f}_0(980)$ resonance (mass, width and amplitude), 2 amplitudes for $\rho(770)^0$ and $\mathrm{f}_2(1270)$ resonances and 4 for f_{bkg}. The masses and widths of $\rho(770)^0$ and $\mathrm{f}_2(1270)$ are well defined in Ref. [1], and those are fixed to $m_\rho = 775.3$ MeV/c^2, $\Gamma_\rho = 149.1$ MeV/c^2, $m_{\mathrm{f}_2} = 1{,}275.5$ MeV/c^2, and $\Gamma_{\mathrm{f}_2} = 186.7$ MeV/c^2 during all fit procedures. Due to the many free parameters in the fit function, the procedure is split into three steps to prevent parameter values to converge in local minima. The purpose of the first step is to obtain unbiased and initial $\mathrm{f}_0(980)$ width. This step is performed using the MB sample over the wider p_{T} range to reduce the effect due to the statistical fluctuations. All the nine parameters are left free. The second step aims at constraining the f_{bkg}. The $\mathrm{f}_0(980)$ width is fixed with the value determined in the previous step. The last fit procedure is processed with the fixed f_{bkg}, while the $\mathrm{f}_0(980)$ width is allowed to vary in the range of $10 < \Gamma_0^{\mathrm{f}_0} < 100$ MeV/c^2. In each step, the amplitudes of the resonances and the mass of the $\mathrm{f}_0(980)$ are left free to vary in the range $0.8 < M_{\pi\pi} < 1.76$ GeV/c^2.

While for the $\mathrm{f}_0(980)$ analysis performed in pp collisions [42] the width is constrained to be 55 MeV/c^2, the present analysis leaves the $\mathrm{f}_0(980)$ width as free parameter. In the previous analysis, no phase space correction was applied. On the other hand, the present analysis considers the phase space correction for possibly larger probability of $\pi\pi$ interference [46] owing to higher multiplicity. It is found that consistent invariant yields are obtained from different analysis methods.

The raw $\mathrm{f}_0(980)$ yields (N_{f_0}) are obtained by integrating the $\mathrm{f}_0(980)$ rBW function in the measured p_{T} range and corrected for the acceptance, the tracking efficiency, and the PID efficiency and then normalized for the event selections and the B.R. [41]. The fully corrected yield can be expressed as

$$\frac{1}{N_{\mathrm{NSD}}}\frac{\mathrm{d}^2N}{\mathrm{d}y\mathrm{d}p_{\mathrm{T}}} = \frac{1}{N_{\mathrm{evt}}}\frac{N_{\mathrm{f}_0}}{\Delta y \Delta p_{\mathrm{T}}}\frac{\varepsilon_{\mathrm{trig}} f_{\mathrm{vtx}} f_{\mathrm{SL}}}{\mathrm{Acc}\times\varepsilon\times\mathrm{B.R.}}. \tag{5}$$

Here, N_{evt} is the number of events satisfying the event selection criteria in the specific multiplicity class. The rapidity interval of 0.5 is represented as Δy. Coefficients for the acceptance (Acc) and the efficiency (ε) of the tracking and PID are estimated from a detailed simulation of the ALICE detector response. The p–Pb events are simulated using the DPMJET [47] event generator with the injection of $\mathrm{f}_0(980)$ signals. Signals and backgrounds are transported through the detector using GEANT3 [48]. The $\mathrm{Acc}\times\varepsilon$ is estimated to be 26% in $0 < p_{\mathrm{T}} < 0.3$ GeV/c interval and gradually increasing up to 60% as p_{T} increases and it is not dependent on the multiplicity class. The B.R. is the branching ratio of the $\mathrm{f}_0(980) \rightarrow \pi^+\pi^-$ decay channel. The $\mathrm{f}_0(980)$ yield is normalized for the trigger efficiency ($\varepsilon_{\mathrm{trig}}$), vertex reconstruction efficiency (f_{vtx}), and signal loss (f_{SL}) due to the event selection. The $\varepsilon_{\mathrm{trig}}$ depends on the multiplicity class increasing from 0.84 to 1 as the multiplicity increases. The f_{vtx} is estimated to be larger than 0.99 in all measured multiplicity classes. Because current realistic simulations do not generate primary $\mathrm{f}_0(980)$, the f_{SL} is estimated using a different particle, the ϕ meson, exploiting the universal m_{T} scaling [49]. This approach shows that f_{SL} does not depend on particle species [30], and it is found to be 1.03 for $0 < p_{\mathrm{T}} < 0.3$ GeV/c and saturates at unity for $p_{\mathrm{T}} > 2$ GeV/c.

4 Systematic uncertainties

The systematic uncertainties of invariant yields are estimated by varying the analysis selection criteria and corrections and are summarised in Tab. 1. The total systematic uncertainty is calculated as the sum in quadrature of the different contributing sources. Each uncertainty does not significantly depend on the chosen p_{T} range and the multiplicity class.

Table 1: The relative systematic uncertainty of invariant p_{T}-differential yields. Numbers given in ranges correspond to minimum and maximum uncertainties.

Sources		Systematic uncertainty (%)
Primary vertex		negligible
Pileup rejection		negligible
Tracking		±4–6
Particle identification		±4–12
Signal extraction	$f_2(1270)$ parameters	±3–9
	$\rho(770)^0$ parameters	±3–8
	Fit range	±0–6
	Initial f_0 width	±2–12
Phase space correction		±3–8
Total (in quadrature)		±15–27

A narrower primary vertex selection is used, $|z_{\mathrm{vtx}}| < 7$ cm, and the variation is estimated to be negligible. The systematic uncertainty from the pileup rejection is tested by varying the minimal number of track segments contributing to the reconstruction of pileup event vertices from 5 to 3. The uncertainty is estimated to be negligible.

The systematic uncertainty from tracking is is taken from [43], where uncertainties are evaluated by varying the requirements to select reconstructed tracks such as d_{xy}, d_z, and the number of fired TPC readout channels. The systematic uncertainty from the particle identification is tested with different requirements on the number of standard deviations ($\pm 0.5\sigma$) for the TPC and TOF. The uncertainties are estimated to be 4–12%.

The contribution coming from masses and widths of $f_2(1270)$ and $\rho(770)^0$ are evaluated by shifting the masses and the widths by plus or minus three unit of their uncertainties from the default value, where uncertainties are reported at Ref [1]. The estimated uncertainties from $f_2(1270)$ and $\rho(770)^0$ parameters are 3–9% and 3–8%, respectively. The systematic uncertainty from the fit range is estimated by changing the range inward or outward by 40 MeV/c^2. The uncertainties are estimated to be less than 6%.

The contribution from the initial guess for the $f_0(980)$ width value, which is obtained in the first step described in Sec. 3, is estimated by varying the width within the statistical uncertainties in both directions. The variations affect the background distribution determined in the second step, and the estimated systematic uncertainties are 2–12%. The systematic uncertainty from phase space correction is estimated by varying the kinetic freeze-out temperature in the range of $140 < T_{\mathrm{kin}} < 180$ MeV. The estimated uncertainties are 3–8%.

The correlations between systematic uncertainties and multiplicity are evaluated by measuring the extent to which uncertainties collectively change. The directional deviations of systematic effects are compared within a given multiplicity class to those observed in the minimum bias (MB) class. It is found that approximately half of the total systematic uncertainties across all sources inspected are uncorrelated and independent of one another.

5 Results

Figure 2 shows the p_{T} spectra of $f_0(980)$ in p–Pb collisions at $\sqrt{s_{\mathrm{NN}}} = 5.02$ TeV measured in the range of $0 < p_{\mathrm{T}} < 8$ GeV/c for different multiplicity classes and non-single diffractive (NSD) events. Each spectrum is scaled with the number denoted in the figure for visibility. The lower panel of Fig. 2 shows the ratios of each p_{T} spectrum to the NSD spectrum. The systematic uncertainties of the ratios are estimated by propagating the multiplicity-uncorrelated uncertainties on the single spectrum. For $p_{\mathrm{T}} < 4$ GeV/c, the hardening of the p_{T} spectrum from low- to high-multiplicity events is clearly seen, while the same shape

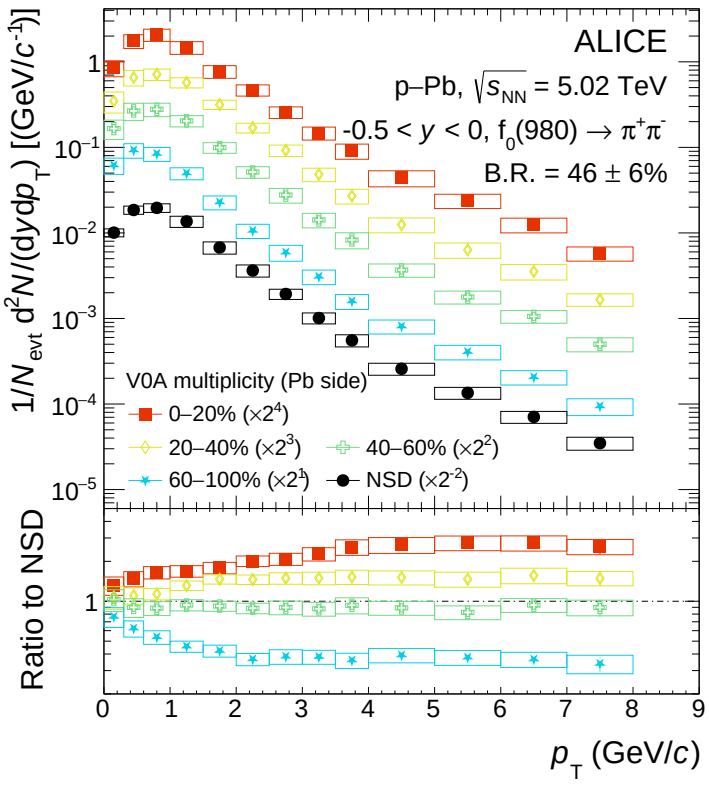

Fig. 2: Transverse momentum spectra of $f_0(980)$ in p–Pb collisions at $\sqrt{s_{NN}}$ = 5.02 TeV for different multiplicity classes, which are scaled for visibility. Statistical and systematic uncertainties are shown as error bars and boxes, respectively. The lower panel shows the ratios of the specific spectra to the NSD spectrum.

is visible at high $p_T > 4$ GeV/c. Such trends can be also observed for other hadronic species [50].

Table 2: The values of dN/dy and mean p_T ($\langle p_T \rangle$) measured in p–Pb collisions at $\sqrt{s_{NN}}$ = 5.02 TeV for different multiplicity classes. The first and second uncertainties represent the statistical and systematic uncertainties, respectively.

Multiplicity class (V0A)	dN/dy	$\langle p_T \rangle$ (GeV/c)
0–20%	0.206±0.005±0.014	1.287±0.034±0.010
20–40%	0.153±0.004±0.010	1.250±0.029±0.082
40–60%	0.113±0.002±0.008	1.142±0.025±0.088
60–100%	0.064±0.001±0.005	0.999±0.014±0.080

Table 2 shows the integrated yield (dN/dy) and mean p_T ($\langle p_T \rangle$) of $f_0(980)$ for different multiplicity classes in p–Pb collisions at $\sqrt{s_{NN}}$ = 5.02 TeV. The dN/dy linearly increases with the multiplicity, while the $\langle p_T \rangle$ concavely increases with the multiplicity.

The left panel of figure 3 shows the double ratios of different particles to charged pion yields as a function of charged-particle multiplicity raised to the power of 1/3 in p–Pb collisions at $\sqrt{s_{NN}}$ = 5.02 TeV. The $\langle dN/d\eta \rangle^{1/3}_{|\eta|<0.5}$ signifies a proxy for the dimensionless size of the system [51]. We use the V0A to select fractions of the visible cross section and to categorize events based on their multiplicity. The systematic uncertainty of the double ratio is calculated considering only the uncorrelated part of the uncertainty. The pion [13], $K^*(892)^0$ [24], and ϕ [24] mesons can be classified according to their lifetimes and to their (anti-) strange quarks. The strangeness enhancement and rescattering effects can be studied by comparing the yield of particles with different characteristics. The ratio of ϕ to π increases with the multiplicity, which is consistent with the observation of the strangeness enhancement [14]. On the other

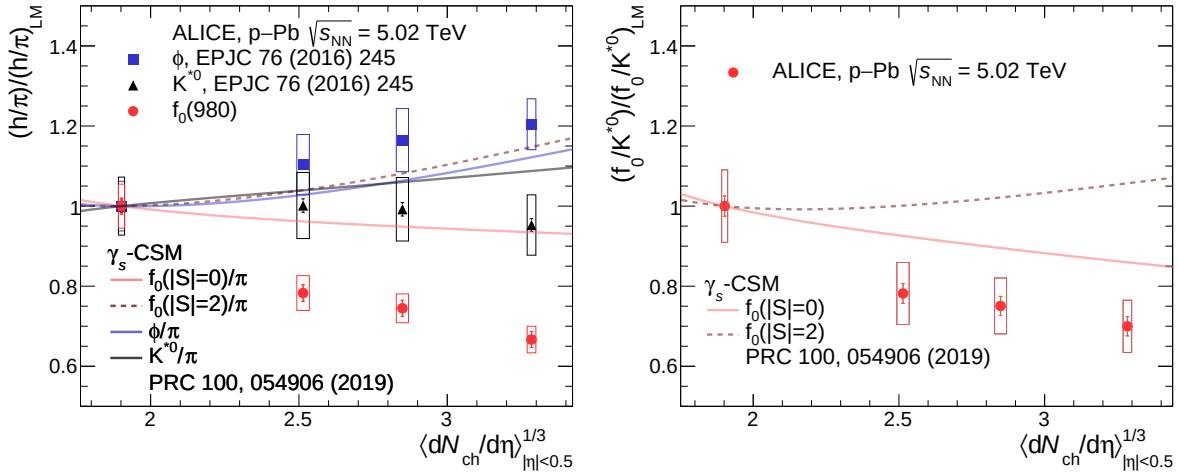

Fig. 3: Double ratios of ϕ [24], $K^*(892)^0$ [24], and $f_0(980)$ to π [13] (left) and $f_0(980)$ to $K^*(892)^0$ (right) as a function of charged-particle multiplicity raised to the power of 1/3. The ratio in each interval is divided by the ratio in low-multiplicity (LM) events to relate the multiplicity dependence to the lowest multiplicity bin and reduce systematic uncertainties. Predictions from the Canonical statistical model are represented with lines.

hand, the ratio of $K^*(892)^0$ to π is flat with the increasing multiplicity even if $K^*(892)^0$ contains one strange quark. The flat trend could be explained by two competing effects, the strangeness enhancement and rescattering effects due to the short lifetime (≈ 4.2 fm/c) of $K^*(892)^0$ [1]. The ratio of $f_0(980)$ to π decreases as the multiplicity increases because of the shorter lifetime of $f_0(980)$, suggesting rescattering effects for $f_0(980)$. Predictions of the ratio of $f_0(980)$ to π are shown in lines for different hidden strangeness assumptions for $f_0(980)$ by γ_s-Canonical Statistical Model (CSM) [52], which considers system-size-dependent hadrochemistry at vanishing baryon density with local conservation of electric charge, baryon density, and strangeness, while allowing for undersaturation of strangeness. Note that γ_s is the parameter for the undersaturation of strangeness derived from measured particle yields. The CSM hypothesis with two hidden strange quarks predicts an increase of the ratio, contrarily to what observed experimentally. Moreover, the CSM with zero hidden strangeness predicts a $f_0(980)$ to π ratio that decreases much less than what measured. Such a difference could be attributed to no rescattering effects in the CSM. The prediction of the CSM for the ratio of ϕ to π nicely reproduces the increasing trend of measured data with the increasing multiplicity, where the hidden strangeness of ϕ is two. However, the CSM overestimates the ratio of $K^*(892)^0$ to π because the modification of $K^*(892)^0$ yields due to rescattering effects are not implemented in the CSM.

The right panel of figure 3 shows the double ratio of $f_0(980)$ to K^{*0} yields as a function of charged-particle multiplicity elevated to 1/3 in p–Pb collisions at $\sqrt{s_{\rm NN}}$ = 5.02 TeV and predictions from the CSM with different hidden strangeness assumptions. The lifetimes of $f_0(980)$ and K^{*0} are estimated to be comparable, indicating that rescattering effects are not expected to be much different. Hence, the ratio is expected to be weakly affected by rescattering effects. The ratio decreases with increasing multiplicity that is qualitatively described with the zero-hidden-strangeness assumption and can be explained by the strangeness enhancement of the K^{*0} yield. The CSM prediction with the two-hidden-strangeness assumptions is mildly increasing as the multiplicity increases, a trend that is opposite to the experimental result as shown in Fig. 3. Therefore, the decreasing trend of the ratio of $f_0(980)$ to K^{*0} can suggest no effective strangeness enhancement for the $f_0(980)$.

Figure 4 shows the $p_{\rm T}$-differential particle yield ratio of $f_0(980)$ to π in high-multiplicity (HM, 0–20%) and low-multiplicity (LM, 60–100%) p–Pb collisions at $\sqrt{s_{\rm NN}}$ = 5.02 TeV. The ratios are consistent within one sigma in $p_{\rm T} > 4$ GeV/c, while the double ratio of HM to LM is suppressed at a lower $p_{\rm T}$ as shown in the lower panel of Fig. 4. In the double ratio, the correlated uncertainties across multiplicity

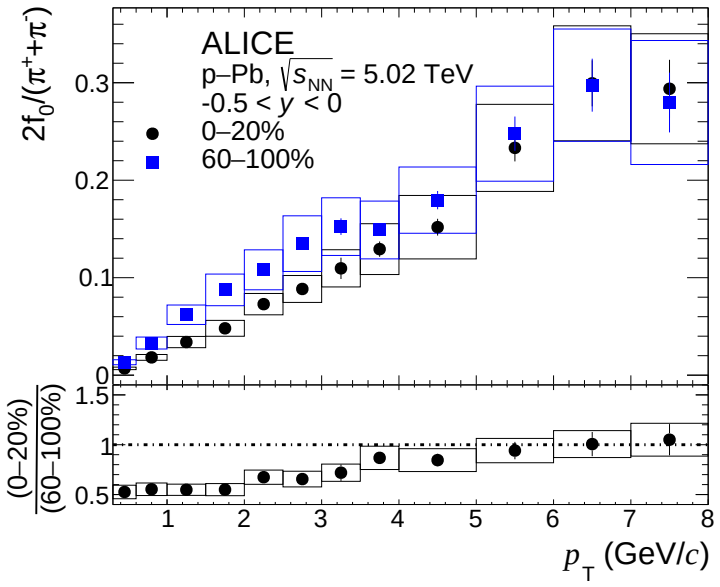

Fig. 4: The particle yield ratios of $f_0(980)$ to π as a function of p_T in high-multiplicity (circles) and low-multiplicity (triangles) p–Pb collisions at $\sqrt{s_{NN}}$ = 5.02 TeV. The lower panel shows the double ratio of $f_0(980)/\pi$ between the high-multiplicity and low-multiplicity events.

classes cancel. The p_T dependence of the double ratio indicates that the suppression of the integrated yield is mainly occurring at low p_T values ($p_T < 4$ GeV/c), which shows the same p_T dependence like the suppression of the K^{*0}/K [23].

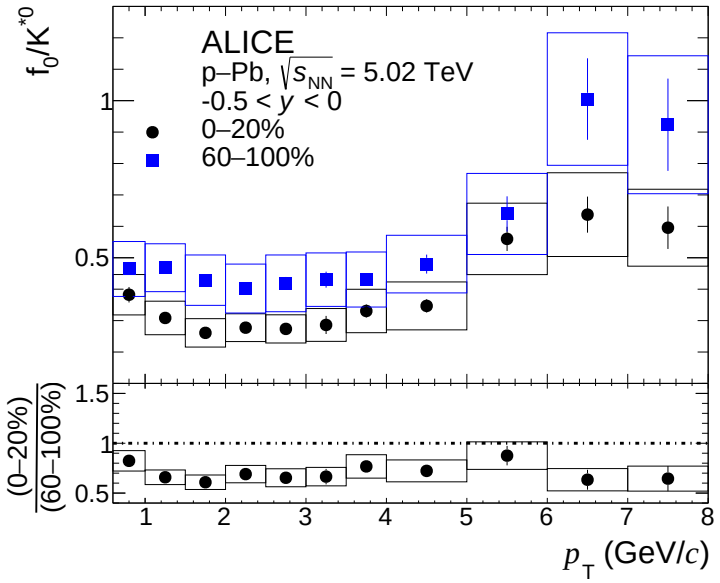

Fig. 5: The particle yield ratio of $f_0(980)$ to $K^{*0}(892)$ as a function of p_T in high-multiplicity (circles) and low-multiplicity (triangles) p–Pb collisions at $\sqrt{s_{NN}}$ = 5.02 TeV. The lower panel shows the double ratio of high-multiplicity to low-multiplicity $f_0(980)/K^{*0}(892)$.

Figure 5 shows p_T-differential particle yield ratio of $f_0(980)$ to K^{*0} in HM and LM p–Pb collisions at $\sqrt{s_{NN}}$ = 5.02 TeV. The ratio from HM events is lower than that of LM events in the entire p_T range, differently from what observed for K^{*0}/K or $f_0(980)/\pi$. The suppression of the ratio of HM events at high p_T indicates that other effects, beyond rescattering effects, are present. For instance, the enhancement of K^{*0} yield due to the strangeness enhancement can explain the suppression over the entire p_T range with

the assumption of no strangeness enhancement for $f_0(980)$. The absence of the strangeness enhancement is inferred as no strange quarks in $f_0(980)$.

As a result, the decreasing trend of the ratio in higher multiplicity events suggests no strange quark in $f_0(980)$.

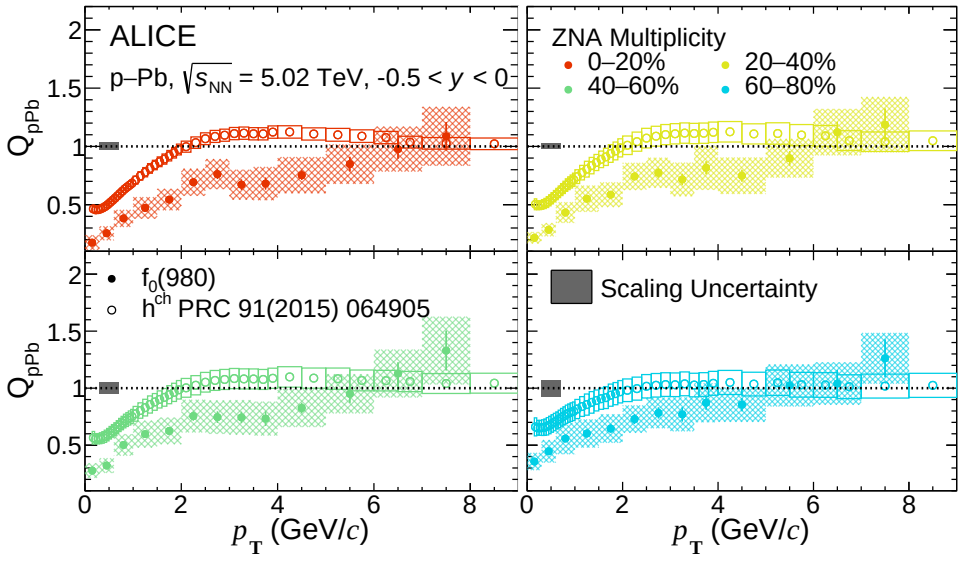

Fig. 6: Nuclear modification factor (Q_{pPb}) of $f_0(980)$ as a function of p_{T} in p–Pb collisions at $\sqrt{s_{\mathrm{NN}}}$ = 5.02 TeV for different multiplicity classes. The multiplicity class is defined with the ZNA, which is the ZN placed at Pb-going side. Statistical and systematic uncertainties are shown as error bars and boxes, respectively. Open boxes around p_{T} = 0.5 GeV/c represent the binary collision scaling uncertainties. The Q_{pPb} of charged hadrons [39] are reported for comparison.

The p_{T}-differential invariant yield of $f_0(980)$in p–Pb collisions can be compared to the one in pp collisions at the same center-of-mass energy by computing the nuclear modification factor Q_{pPb}, defined as

$$Q_{\mathrm{pPb}} = \frac{\mathrm{d}^2 N^{\mathrm{pPb}}_{\mathrm{f_0(980)}}/\mathrm{d}p_{\mathrm{T}}\mathrm{d}y}{\langle T_{\mathrm{pPb}}\rangle \, \mathrm{d}^2\sigma^{\mathrm{pp}}_{\mathrm{f_0(980)}}/\mathrm{d}p_{\mathrm{T}}\mathrm{d}y}, \tag{6}$$

where $\langle T_{\mathrm{pPb}}\rangle$ and $\sigma^{\mathrm{pp}}_{\mathrm{f_0(980)}}$ are extracted using an event selection based on the ZN to minimize the possible biases according to what reported in [39] and the cross section for the production of $f_0(980)$ in pp collisions measured and reported in [42], respectively. Note that the B.R. is cancelled out in the measurement of the Q_{pPb} as the same value is used in pp and p–Pb collisions.

Figure 6 shows the Q_{pPb} of $f_0(980)$ in p–Pb collisions at $\sqrt{s_{\mathrm{NN}}}$ = 5.02 TeV in different multiplicity classes. The Pb-remnant side neutron calorimeter, labeled ZNA, is used to select centrality intervals to calculate the Q_{pPb}. The systematic uncertainties are calculated with the assumption that there is no correlated uncertainty between the yield in pp and p–Pb collisions. The $f_0(980)$ is getting more suppressed than charged hadrons [39] for $p_{\mathrm{T}} < 4$ GeV/c with increasing multiplicity. As p_{T} increases, $f_0(980)$ Q_{pPb} values become compatible with those for charged particles, reaching unity. The dependencies of the nuclear modification factor on the multiplicity and p_{T} are the same as observed in Fig. 4, indicating rescattering effects largely contribute to the suppression of the $f_0(980)$ yield. In addition, the Q_{pPb} does not exhibit Cronin peak [19] at the intermediate p_{T} in HM events. This is consistent trend of conventional mesons [13]. The absence of Cronin peak for $f_0(980)$ might suggests that the number of constituent quarks of $f_0(980)$ is smaller than three.

6 Conclusions

The multiplicity dependent $f_0(980)$ production in p–Pb collisions at $\sqrt{s_{NN}}$ = 5.02 TeV is presented. The $f_0(980)$ is reconstructed via the $f_0(980) \rightarrow \pi^+\pi^-$ decay channel in midrapidity ($-0.5 < y < 0$) in a transverse momentum region of $0 < p_T < 8$ GeV/c. The p_T spectra of $f_0(980)$ particles show an increasing trend of the yield and the mean p_T for higher multiplicity events. The particle yield ratio of $f_0(980)$ to π is decreasing with increasing multiplicities, and the suppression of the $f_0(980)$ to π ratio is observed only at low $p_T < 4$ GeV/c, indicating that the rescattering effects exist for $f_0(980)$ particles. The Canonical Statistical Model (CSM) overestimates the $f_0(980)/\pi$ and it does not describe the decreasing trend because the CSM does not consider rescattering effects. The particle yield ratio of $f_0(980)$ to K^{*0} also decreases with increasing multiplicities. The suppression of the $f_0(980)$ to K^{*0} ratio is observed in the entire p_T region, showing a different p_T dependency relative to the one expected from a rescattering scenario. The CSM qualitatively estimates the decreasing trend for $f_0(980)/K^{*0}$ with the assumption of no hidden strangeness for $f_0(980)$, while it overestimates the $f_0(980)/K^{*0}$ with the assumption of the two hidden strangeness. The result implies that K^{*0} is relatively enhanced compared with $f_0(980)$ due to the strangeness enhancement. Furthermore, the multiplicity-dependent nuclear modification factor for $f_0(980)$ exhibits a strong suppression at a low p_T and the suppression depends on the multiplicity class, which can be explained by the rescattering effects. Additionally, no Cronin peak is observed from the nuclear modification factor, even in high-multiplicity events. This suggests that the number of constituent quarks of the $f_0(980)$ particle is smaller than three.

Acknowledgements

References

[1] **Particle Data Group** Collaboration, R. L. Workman *et al.*, "Review of Particle Physics", *PTEP* **2022** (2022) .

[2] **ExHIC** Collaboration, S. Cho *et al.*, "Multi-quark hadrons from Heavy Ion Collisions", *Phys. Rev. Lett.* **106** (2011) , arXiv:1011.0852 [nucl-th].

[3] R. L. Jaffe, "Multi-Quark Hadrons. 1. The Phenomenology of (2 Quark 2 anti-Quark) Mesons", *Phys. Rev. D* **15** (1977) .

[4] L. Maiani, F. Piccinini, A. D. Polosa, and V. Riquer, "A New look at scalar mesons", *Phys. Rev. Lett.* **93** (2004) , arXiv:hep-ph/0407017.

[5] C.-H. Chen, "Evidence for two quark content of f(0)(980) in exclusive b —> c decays", *Phys. Rev. D* **67** (2003) , arXiv:hep-ph/0302059.

[6] N. N. Achasov, J. V. Bennett, A. V. Kiselev, E. A. Kozyrev, and G. N. Shestakov, "Evidence of the four-quark nature of $f_0(980)$ and $f_0(500)$", *Phys. Rev. D* **103** no. 1, (2021) , arXiv:2009.04191 [hep-ph].

[7] H. A. Ahmed and C. W. Xiao, "Study the molecular nature of σ, $f_0(980)$, and $a_0(980)$ states", *Phys. Rev. D* **101** no. 9, (2020) , arXiv:2001.08141 [hep-ph].

[8] R. S. Bhalerao, "Collectivity in large and small systems formed in ultrarelativistic collisions", *Eur. Phys. J. ST* **230** no. 3, (2021) , arXiv:2009.09586 [nucl-th].

[9] **ALICE** Collaboration, S. Acharya *et al.*, "Investigations of Anisotropic Flow Using Multiparticle Azimuthal Correlations in pp, p-Pb, Xe-Xe, and Pb-Pb Collisions at the LHC", *Phys. Rev. Lett.* **123** no. 14, (2019) , arXiv:1903.01790 [nucl-ex].

[10] **ALICE** Collaboration, S. Acharya *et al.*, "Measurements of inclusive jet spectra in pp and central Pb-Pb collisions at $\sqrt{s_{\rm NN}}$ = 5.02 TeV", *Phys. Rev. C* **101** no. 3, (2020) , arXiv:1909.09718 [nucl-ex].

[11] **ALICE** Collaboration, S. Acharya *et al.*, "Production of charged pions, kaons, and (anti-)protons in Pb-Pb and inelastic pp collisions at $\sqrt{s_{NN}}$ = 5.02 TeV", *Phys. Rev. C* **101** no. 4, (2020) , arXiv:1910.07678 [nucl-ex].

[12] **STAR** Collaboration, J. Adams *et al.*, "Experimental and theoretical challenges in the search for the quark gluon plasma: The STAR Collaboration's critical assessment of the evidence from RHIC collisions", *Nucl. Phys.* **A757** (2005) , arXiv:nucl-ex/0501009 [nucl-ex].

[13] **ALICE** Collaboration, J. Adam *et al.*, "Multiplicity dependence of charged pion, kaon, and (anti)proton production at large transverse momentum in p-Pb collisions at $\sqrt{s_{\rm NN}}$ = 5.02 TeV", *Phys. Lett. B* **760** (2016) , arXiv:1601.03658 [nucl-ex].

[14] **ALICE** Collaboration, J. Adam *et al.*, "Enhanced production of multi-strange hadrons in high-multiplicity proton-proton collisions", *Nature Phys.* **13** (2017) , arXiv:1606.07424 [nucl-ex].

[15] **PHENIX** Collaboration, C. Aidala *et al.*, "Creation of quark–gluon plasma droplets with three distinct geometries", *Nature Phys.* **15** no. 3, (2019) , arXiv:1805.02973 [nucl-ex].

[16] **ALICE** Collaboration, S. Acharya *et al.*, "Long- and short-range correlations and their event-scale dependence in high-multiplicity pp collisions at $\sqrt{s} = 13$ TeV", *JHEP* **05** (2021) , arXiv:2101.03110 [nucl-ex].

[17] **LHCb** Collaboration, R. Aaij *et al.*, "Measurement of resonant and CP components in $\bar{B}^0_s \to J/\psi\pi^+\pi^-$ decays", *Phys. Rev. D* **89** no. 9, (2014) , arXiv:1402.6248 [hep-ex].

[18] **LHCb** Collaboration, R. Aaij *et al.*, "Measurement of the resonant and CP components in $\overline{B}^0 \to J/\psi\pi^+\pi^-$ decays", *Phys. Rev. D* **90** no. 1, (2014) , arXiv:1404.5673 [hep-ex].

[19] J. W. Cronin, H. J. Frisch, M. J. Shochet, J. P. Boymond, R. Mermod, P. A. Piroue, and R. L. Sumner, "Production of hadrons with large transverse momentum at 200, 300, and 400 GeV", *Phys. Rev. D* **11** (1975) .

[20] R. J. Fries, B. Muller, C. Nonaka, and S. A. Bass, "Hadronization in heavy ion collisions: Recombination and fragmentation of partons", *Phys. Rev. Lett.* **90** (2003) , arXiv:nucl-th/0301087.

[21] M. Wang, J.-Q. Tao, H. Zheng, W.-C. Zhang, L.-L. Zhu, and A. Bonasera, "Number-of-constituent-quark scaling of elliptic flow: a quantitative study", *Nucl. Sci. Tech.* **33** no. 3, (2022) , arXiv:2203.10353 [hep-ph].

[22] **ALICE** Collaboration, S. Acharya *et al.*, "Production of the $\rho(770)^0$ meson in pp and Pb-Pb collisions at $\sqrt{s_{\rm NN}}$ = 2.76 TeV", *Phys. Rev. C* **99** no. 6, (2019) , arXiv:1805.04365 [nucl-ex].

[23] **ALICE** Collaboration, S. Acharya *et al.*, "Multiplicity dependence of K*$(892)^0$ and $\phi(1020)$ production in pp collisions at $\sqrt{s}$ =13 TeV", *Phys. Lett. B* **807** (2020) , arXiv:1910.14397 [nucl-ex].

[24] **ALICE** Collaboration, J. Adam *et al.*, "Production of K* $(892)^0$ and ϕ (1020) in p–Pb collisions at $\sqrt{s_{\rm NN}}$ = 5.02 TeV", *Eur. Phys. J. C* **76** no. 5, (2016) , arXiv:1601.07868 [nucl-ex].

[25] **ALICE** Collaboration, "$\Sigma(1385)^{\pm}$ resonance production in Pb-Pb collisions at $\sqrt{s_{\rm NN}} = 5.02$ TeV", arXiv:2205.13998 [nucl-ex].

[26] **ALICE** Collaboration, S. Acharya *et al.*, "Suppression of $\Lambda(1520)$ resonance production in central Pb-Pb collisions at $\sqrt{s_{\rm NN}}$ = 2.76 TeV", *Phys. Rev. C* **99** (2019) , arXiv:1805.04361 [nucl-ex].

[27] C. Bierlich, T. Sjöstrand, and M. Utheim, "Hadronic rescattering in pA and AA collisions", *Eur. Phys. J. A* **57** no. 7, (2021) , arXiv:2103.09665 [hep-ph].

[28] C. Song and V. Koch, "Chemical relaxation time of pions in hot hadronic matter", *Phys. Rev. C* **55** (1997) , arXiv:nucl-th/9611034.

[29] **ALICE** Collaboration, K. Aamodt *et al.*, "Two-pion Bose-Einstein correlations in central Pb-Pb collisions at $\sqrt{s_{NN}} = 2.76$ TeV", *Phys. Lett. B* **696** (2011) , arXiv:1012.4035 [nucl-ex].

[30] **ALICE** Collaboration, S. Acharya *et al.*, "Evidence of rescattering effect in Pb-Pb collisions at the LHC through production of K$^*(892)^0$ and $\phi(1020)$ mesons", *Phys. Lett. B* **802** (2020) , arXiv:1910.14419 [nucl-ex].

[31] **ALICE** Collaboration, S. Acharya *et al.*, "Multiplicity dependence of light-flavor hadron production in pp collisions at $\sqrt{s}$ = 7 TeV", *Phys. Rev. C* **99** no. 2, (2019) , arXiv:1807.11321 [nucl-ex].

[32] **ALICE** Collaboration, B. B. Abelev *et al.*, "Performance of the ALICE Experiment at the CERN LHC", *Int. J. Mod. Phys.* **A29** (2014) , arXiv:1402.4476 [nucl-ex].

[33] **ALICE** Collaboration, E. Abbas *et al.*, "Performance of the ALICE VZERO system", *JINST* **8** (2013) , arXiv:1306.3130 [nucl-ex].

[34] **ALICE** Collaboration, P. Cortese, "Performance of the ALICE Zero Degree Calorimeters and upgrade strategy", *J. Phys. Conf. Ser.* **1162** no. 1, (2019) .

[35] **ALICE** Collaboration, K. Aamodt *et al.*, "Alignment of the ALICE Inner Tracking System with cosmic-ray tracks", *JINST* **5** (2010) , arXiv:1001.0502 [physics.ins-det].

[36] J. Alme *et al.*, "The ALICE TPC, a large 3-dimensional tracking device with fast readout for ultra-high multiplicity events", *Nucl. Instrum. Meth. A* **622** (2010) , arXiv:1001.1950 [physics.ins-det].

[37] **ALICE** Collaboration, N. Jacazio, "PID performance of the ALICE-TOF detector at Run 2", *PoS* **LHCP2018** (2018) , arXiv:1809.00574 [physics.ins-det].

[38] **ALICE** Collaboration, B. B. Abelev *et al.*, "Measurement of visible cross sections in proton-lead collisions at $\sqrt{s_{\rm NN}}$ = 5.02 TeV in van der Meer scans with the ALICE detector", *JINST* **9** no. 11, (2014) , arXiv:1405.1849 [nucl-ex].

[39] **ALICE** Collaboration, J. Adam *et al.*, "Centrality dependence of particle production in p-Pb collisions at $\sqrt{s_{\rm NN}}$= 5.02 TeV", *Phys. Rev. C* **91** no. 6, (2015) , arXiv:1412.6828 [nucl-ex].

[40] R. Santoro *et al.*, "The ALICE Silicon Pixel Detector: Readiness for the first proton beam", *JINST* **4** (2009) .

[41] S. Stone and L. Zhang, "Use of $B \to J/\psi f_0$ decays to discern the $q\bar{q}$ or tetraquark nature of scalar mesons", *Phys. Rev. Lett.* **111** no. 6, (2013) , arXiv:1305.6554 [hep-ex].

[42] **ALICE** Collaboration, "$\mathrm{f}_0(980)$ production in inelastic pp collisions at $\sqrt{s} = 5.02$ TeV", arXiv:2206.06216 [nucl-ex].

[43] **ALICE** Collaboration, B. B. Abelev *et al.*, "Multiplicity Dependence of Pion, Kaon, Proton and Lambda Production in p-Pb Collisions at $\sqrt{s_{NN}}$ = 5.02 TeV", *Phys. Lett. B* **728** (2014) , arXiv:1307.6796 [nucl-ex].

[44] T. Sjöstrand and M. van Zijl, "A multiple-interaction model for the event structure in hadron collisions", *Phys. Rev. D* **36** (Oct, 1987) . https://link.aps.org/doi/10.1103/PhysRevD.36.2019.

[45] **OPAL** Collaboration, K. Ackerstaff *et al.*, "Photon and light meson production in hadronic Z0 decays", *Eur. Phys. J. C* **5** (1998) , arXiv:hep-ex/9805011.

[46] **STAR** Collaboration, J. Adams *et al.*, "Rho0 production and possible modification in Au+Au and p+p collisions at S(NN)**1/2 = 200-GeV", *Phys. Rev. Lett.* **92** (2004) , arXiv:nucl-ex/0307023.

[47] A. Fedynitch, *Cascade equations and hadronic interactions at very high energies*. PhD thesis, KIT, Karlsruhe, Dept. Phys., 11, 2015.

[48] R. Brun, F. Bruyant, F. Carminati, S. Giani, M. Maire, A. McPherson, G. Patrick, and L. Urban, "GEANT Detector Description and Simulation Tool",.

[49] L. Altenkämper, F. Bock, C. Loizides, and N. Schmidt, "Applicability of transverse mass scaling in hadronic collisions at energies available at the CERN Large Hadron Collider", *Phys. Rev. C* **96** no. 6, (2017) , arXiv:1710.01933 [hep-ph].

[50] C. Tsallis, "Possible Generalization of Boltzmann-Gibbs Statistics", *J. Statist. Phys.* **52** (1988) .

[51] P. Liu and R. A. Lacey, "System-size dependence of the viscous attenuation of anisotropic flow in p + Pb and Pb + Pb collisions at energies available at the CERN Large Hadron Collider", *Phys. Rev. C* **98** no. 3, (2018) , arXiv:1804.04618 [nucl-ex].

[52] V. Vovchenko, B. Dönigus, and H. Stoecker, "Canonical statistical model analysis of p-p , p -Pb, and Pb-Pb collisions at energies available at the CERN Large Hadron Collider", *Phys. Rev. C* **100** no. 5, (2019) , arXiv:1906.03145 [hep-ph].